ELSEVIER

International Journal of Mass Spectrometry 197 (2000) 71–84

International Journal of Mass Spectrometry

Generation of metal–ligand cluster ion beams through pulsed discharge ionization and ablation

Ansgar Brock, David L. Cedeño, Carlos Manzanares I.*

Department of Chemistry, Baylor University, Waco, TX 76798, USA

Received 10 November 1998; accepted 30 July 1999

Abstract

Pulsed capacitor discharge ionization in supersonic expansions was investigated for the production of intense beams of molecular cluster ions from seeded and ablated compounds. A pulsed discharge based on a triggered spark gap switch was designed and used as a method for ionization and ablation. Several combinations of nozzle geometry and electrode arrangement in front of a pulsed valve, were made to optimize the intensity of the ion beam as well as its composition. The cationic metal–ligand complexes Cu^+–(methanol)$_n$, Cu^+–(acetone)$_n$, Cu^+–(toluene)$_n$, Cu^+–(water)$_n$, and Al^+–(water)$_n$ were synthesized by ablation of the metal from metallic discharge electrodes in a discharge gas mixture of helium seeded with the ligand of choice. The cluster mass spectra of the expanded plasmas show little background ion signal besides the metal–ligand species. Charge exchange processes in the expansion guarantee high ionization yields of the desired species and account for low backgrounds. Changes in the successive binding energy of Cu^+–(water)$_n$ clusters $n = 1$–4 are clearly observed in the cluster mass spectra as step formation. A similar pattern found in Cu^+–(acetone)$_n$ suggests the same trend in the successive binding energy as known for water. (Int J Mass Spectrom 197 (2000) 71–84) © 2000 Elsevier Science B.V.

Keywords: Pulsed discharge; Cluster ions; Time-of-flight mass spectrometry

1. Introduction

The method of laser ablation and ionization in supersonic expansions was introduced by Dietz et al. [1] and by Bondybey and English [2]. One laser can accomplish ablation and ionization [3], but most of the time two lasers are employed [4], one for ablation and another one for ionization after the supersonic expansion. The source of atoms or ions consists of a rotating rod or disc of the material to be ablated. The material is in contact with the expansion gas streaming through the expansion channel. The laser (typically 10 ns pulse width, 20 mJ per pulse [5]) hits the target through a window, which is installed on the other side of the channel. The high peak power of the laser ablates about 500 atomic layers per shot. A plasma of 10 000–20 000 K results.

As an alternative to the laser ablation method, the pulsed arc cluster ion source (PACIS) [6,7] was developed. The PACIS accomplishes two tasks, namely the ablation of the material to be clustered from the electrodes of arc discharge and its ionization in the expanding arc plasma. The arc is generated by a thyristor fired capacitor discharge in the expansion

* Corresponding author. E-mail: Carlos_Manzanares@baylor.edu

PII S1387-3806(99)00168-2

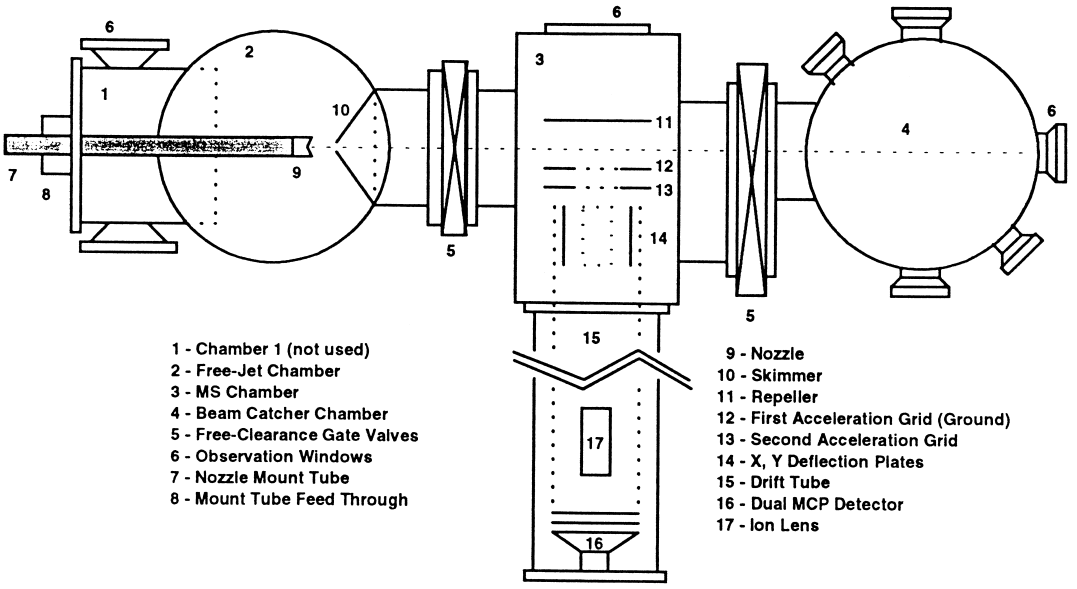

Fig. 1. Molecular beam apparatus.

channel of a pulsed nozzle. Capacitances up to 23 μF and voltages in the range 300–1200 V are used. Metal cluster anions leaving the source are found to carry 10% of the ablated electrode material. If large power inputs into the discharge are introduced, PACIS [6] allows one to create more intense metal cluster ion beams than with the usually employed laser desorption ionization source. The disadvantages are the requirement of source cooling, a mixing chamber after the arc, and a long expansion channel.

In this article, we report the use of pulsed capacitor discharge ionization in a supersonic expansion for the production of intense beams of metal–ligand cluster ions from seeded and ablated compounds. We will show that the requirements mentioned for PACIS are not necessary for the production of metal–ligand clusters. Only small quantities of metal need to be ablated because supersaturation of metal vapor does not need to be achieved as is the case for condensation of pure metal clusters.

A pulsed discharge based on a triggered spark gap switch was designed and used as a method for ionization and ablation. Several combinations of nozzle geometry and electrode arrangement in front of a pulsed valve were made in order to optimize the intensity of the ion beam as well as its composition. The cationic metal–ligand complexes Cu^+–(methanol)$_n$, Cu^+–(acetone)$_n$, Cu^+–(toluene)$_n$, Cu^+–(water)$_n$, and Al^+–(water)$_n$ were synthesized by ablation of the metal from metallic discharge electrodes in a discharge gas mixture of helium seeded with the ligand of choice.

2. Experimental

2.1. Molecular beam apparatus

Fig. 1 shows the apparatus which consists of four vacuum chambers and a time-of-flight mass spectrometer (TOF-MS). Chamber 1 is inserted in a teelike fashion into the free-jet chamber [2]. Chambers 1 and 4 were not used in the present experimental setup. The background pressure in the system was 5×10^{-7} Torr.

The TOF-MS is a commercially available linear instrument from Comstock, Inc. (Model TOF-101). The ion source (Comstock, TFEG/400) is of two stage Wiley-McLaren design with an electron gun as a ionization source. The electron gun of the TOF-MS

was only used for calibration purposes. The static voltages to the flight tube, the deflection plates, the ion lens and the detector are supplied by a single power supply (Comstock, TFP-101). The repeller is powered by a power supply (Comstock, RPS-112) coupled to a pulse forming module (EPC, PG450p). The detector is a dual microchannel plate arranged in a chevron configuration.

The ion source of the TOF-MS was adapted for acceptance of an external ion beam. This was done by fixing a holder to it which is electrically isolated from the repeller and connected with the electron gun ground. The holder was made from a piece of sheet aluminum and dimensioned to cover the back of the repeller as well as the entrance side of the molecular beam. Most of the time only a large piece of wire mesh was attached to it. This was necessary to shield against fringe fields from the flight tube. With a flight tube potential of −5 kV, severe deflection of the ion beam without the shield was observed.

The sample seed system consisted of a carrier gas coming from a cylinder which was split into a bypass and a trap stream. The ratio of the two streams was regulated with needle valves inserted into the lines. Only a fraction of the carrier was seeded with the sample by bubbling it through the trap containing the pure sample. The major part of the gas usually bypassed through the bypass line. Both streams recombined and mixed on their way to the nozzle. There was no need for a special mixing device, because the length of tubing leading to the nozzle is more than 1 m and has an inner diameter of only 2 mm. The gas mixture was flushed through the molecular beam valve. Although flow through the nozzle determines the rate, the unused gas does not go back to the trap. Instead, it leaves through a dump line, which is closer to the nozzle.

2.2. Pulsed discharge ionization source

A pulsed discharge ionization source was built in our laboratory to produce metal–ligand ion beams. The pulser employing a serial spark gap arrangement is shown in Fig. 2. Serial spark gap means that the trigger spark gap (SG2) and the ionizer spark gap

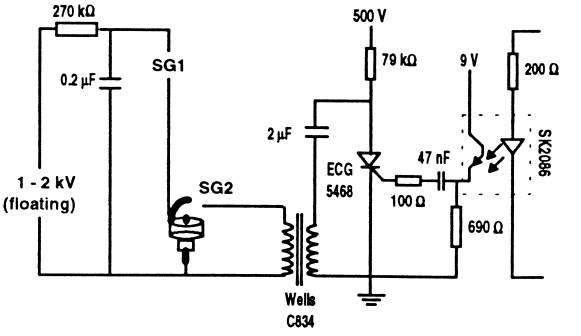

Fig. 2. Schematics of the spark gap pulser circuit in serial configuration (SG1 = ionizer spark gap and SG2 = trigger spark gap).

(SG1) are in series with respect to the applied charging voltage. The high voltage is applied across both gaps. A floating or grounded power supply charges the energy storage capacitor to full potential. SG1 is located in front of the nozzle head piece. The electrodes of the ionizer are of varying shapes and are discussed in Sec. 2.3.

The charging of the energy storage capacitor (0.2 μF) occurs through a 270 kW resistor from a dc HV power supply (NJE Corp., Model WR5E). In the absence of SG2, SG1 can break down if the storage capacitor is charged to more than about 500 V and gas from the nozzle flows in between the electrodes. However, the break down does not occur because SG2 provides the additional insulation needed to prevent break down.

Trigger pulses are supplied by a digital delay generator (SRS, DG 535). To protect the delay generator against any surge currents, it is isolated from the trigger circuit by an opto isolator (SK 2086, 7.5 kV protection). This became necessary after the outputs of the delay generator got damaged repeatedly in normal operation. The trigger pulse is coupled to the gate of a thyristor (ECG 5468). The firing of the thyristor by the gate pulse discharges a 2 mF capacitor charged to 500 V through the primary of an ignition coil (Wells C834).

When the automotive ignition coil delivers a spark to one of the spark plug electrodes near the gap, the gap becomes conductive and the full potential of the

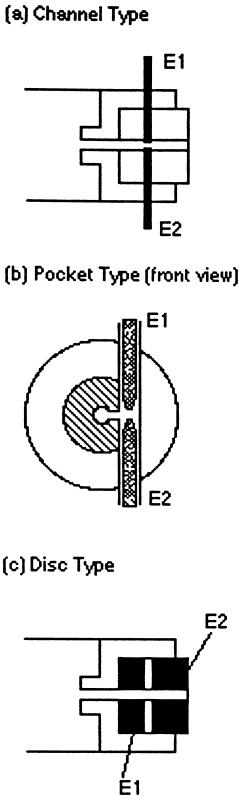

Fig. 3. Schematics of several nozzle shapes and electrode arrangements.

energy storage capacitor is applied to the ionizer gap. This breaks the ionizer gap down and closes the discharge circuit. The series spark gap worked for voltages up to 2 kV.

2.3. Nozzle shapes and electrode arrangements

In the process of optimizing the intensity of the ion beam as well as its composition, a number of changes in the nozzle geometry and the electrode arrangement were made. This involved basically the change of the support piece inserted into the holder rim in front of the molecular beam valve (General Valve Inc.). Next, various inserts are described with remarks about their performance. The inserts are shown in Fig. 3(a)–(c).

The channel-type nozzle is shown in Fig. 3(a). In this nozzle, the discharge is located inside the expansion channel. Ionization can occur before and during the expansion. Two electrodes of 1 mm diameter are positioned across a 2 mm expansion channel insulated from each other by glass capillary tubes that surround the inserted electrodes. The spacing of the discharge electrodes can be varied from 1 to 5 mm. This arrangement performed best for the production of metal–ligand clusters, where the metal was sputtered from the electrodes. Ion signals decrease as the length of the expansion channel following the electrodes increases. This is due to an increasing recombination of the plasma with channel length.

The pocket-type nozzle is shown in Fig. 3(b). The discharge volume is separated from the expansion channel by locating it in a pocket to the right side of the line of expansion of the jet. The discharge volume is connected to the expansion volume by a hole to the side of the expansion channel. Signal levels are lower when compared to nozzle in Fig. 3(a). The discharge was found to become erratic after several hours of operation. Deposits of sputtered material on the walls of the discharge pocket seem to partially short the discharge. This type of discharge worked well for the synthesis of copper–water clusters but not for other metal–ligand clusters.

The disc-type nozzle is shown in Fig. 3(c). Disc-type nozzles were made from two cylindrical electrodes and insulating spacers. The insulator was made from a 2 mm thick peace of borosilicate glass cut from a peace of capillary tubing or from 1-mm-thick polyethylene. The cylindrical electrodes varied in length from a millimeter up to a centimeter. The nozzle was easy to manufacture and performed similar to the channel-type nozzle. Sputtering was not observed to be very efficient with this type of electrode. Marked polarity effects are observed in this electrode arrangement. The field strength in the short channel between the electrodes is very high. Cations are prevented from exiting the nozzle if the front electrode is connected to large positive voltages.

2.4. Timing sequence

A typical timing sequence for discharge ionization is given next. The internal trigger source of the digital

delay generator (SRS, DG 535) sets the repetition rate of the experiment, typically 1 or 2 Hz. At $t = 0$ the output of the delay generator connected to the nozzle driver sends a pulse to open the nozzle. Around 400 μs later, the ionizer discharge circuit receives a trigger edge from the generator. The exact delay depends on the discharge voltage, electrode spacing, and spark–gap distance. The discharge stays on for a few microseconds before it ceases. The on time depends on the size and type of the discharge capacitors.

It takes around 280 μs for the ion packet to travel the 40 cm distance from the nozzle to the extraction region of the TOF-MS. Therefore, the repeller is typically pulsed 300 μs after the discharge trigger to initiate ion extraction from the source region of the TOF-MS. The delay of the repeller is offset on the discharge trigger.

The oscilloscope is triggered around 1 μs after the repeller to compensate for delays in the circuitry of the repeller pulser power supply. This is done to keep the offset in the flight times within a few nanoseconds with respect to $t = 0$ of the data acquisition time. The acquisition of a single shot spectrum is done in less than 100 μs. However, the obtained mass spectra are averages of approximately 300 discharge pulses. Given that the pulse rate is generally 1 Hz, the total acquisition time is 5 min.

3. Results and discussion

3.1. Solvated metal–ion clusters

Different approaches have been used to generate metal ions and to study their reactions with neutral molecules. Laser ablation [8–12], thermionic emission [13], and fast atom bombardment [14] have been used to produce the metal ions. The spectroscopy and structure of metal ion–solvent have been studied previously for some solvated metal ions in the gas phase [15–24]. The effects of solvation are indirectly inferred from the measured photodissociation spectra and fragmentation products.

The mass spectra presented in this section were acquired following the general experimental procedure described above. The Cu and Al ions used for the synthesis of the metal–ligand clusters were generated by ablating or sputtering of electrode material during the discharge. The discharge pulse was generated with the serial spark gap pulser built in our laboratory. Changes in the nozzle geometry and the electrode arrangement were made to synthesize different metal ligand clusters. This involved basically the change of the support piece inserted into the holder rim in front of the molecular beam valve. Next, some of the metal–ligand clusters, as well as the electrode arrangements used in each synthesis will be discussed. A comparison is also made between our results using a discharge ionization source and the mass spectra obtained with other methods.

3.2. Copper with methanol

A mass spectrum of Cu^+–$(CH_3OH)_n$ complexes is shown in Fig. 4. The mass spectrum was obtained using the channel-type nozzle of Fig. 3(a) with a copper cathode and graphite anode. The discharge was done with a 0.2 μF capacitor charged to 1 kV. The concentration of methanol seeded in helium was 13% with a backing pressure of 1 atm. The doublet of the ^{63}Cu and ^{65}Cu isotopes is visible. Complexes up to $n = 3$ are observed and in all complexes the doublet structure, due to the copper isotope distribution, is recognized. A small feature at 91, 92, and 93 u is due to a toluene impurity from a previous experiment. A very small peak occurs at 81 u and another feature at 113 u. The difference in mass between these is 32 u, the molecular mass of methanol. The two features are therefore most likely interrelated by the addition of a methanol molecule to the small cluster. The 81 u feature is most likely the Cu^+–(H_2O) complex, due to the difference of 18 u to Cu^+. This seems to be confirmed by the observable copper doublet, which can only be recognized on an expanded intensity scale.

The amount of methanol seeded into helium was 13% (quite large), but still only small clusters are observed. It can be assumed that most of the methanol in the expansion is lost by self-association to form

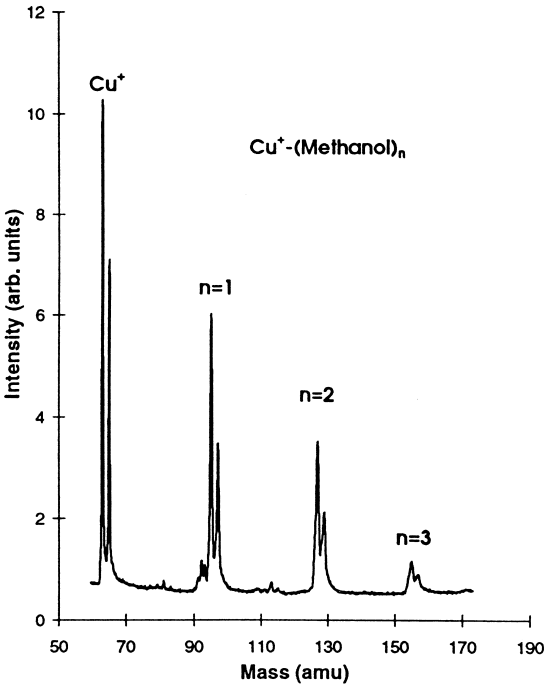

Fig. 4. Cluster mass spectrum of Cu^+–(methanol)$_n$. The ligated metal ion peaks corresponding to $n = 1$, 2, and 3 are the major features besides the Cu^+ isotopes at 63 and 65 u. Toluene impurity peaks are also observed. Expansion conditions: 13% methanol in He, backing pressure 1 atm, channel-type nozzle [Fig. 3(a)] with Cu cathode and graphite anode, discharge 0.2 μF/1 kV.

large clusters. There is no evidence of pure or protonated ligand clusters in the copper–methanol spectra.

The ionization potential of CH_3OH is 10.8 eV. In the adduct complex, charge exchange interaction will not be expected to contribute significantly to the bonding. In reaction studies of Cu^+ with alcohols in the gas phase, hydride and methide abstraction have been observed, but methanol was found to form the adduct complex exclusively [14]. The observed Cu^+–$(CH_3OH)_n$ complexes are expected to be exclusively adductive in nature.

Our results compare well with those obtained by Weil and Wilkins [11] using laser ablation. They found that methanol and copper (I) only react to form the condensation products Cu^+–$(CH_3OH)_n$. They did not report, however, the extent of the condensation. El-Shall et al. [12] report copper–methanol ions where 1–3 methanol molecules are attached to the metal ion. Although no direct comparison with their mass spectrum is possible, there is an agreement to the extent of the clustering. They also obtained apparent binding enthalpies which indicate that the binding energy of the second methanol molecule is slightly larger than that for the first molecule. Kaya et al. [25] have found an intensity gap in going from $n = 2$ to $n = 3$ for ion clusters of methanol and magnesium and vanadium ions. They associated their cluster distribution to a drop in the binding enthalpy beyond the attachment of a second ligand. The same kind of results have been found for copper hydrates and copper ammonium clusters [14,26,27]. We have observed a similar intensity gap in our copper–methanol spectra. The intensity ratio in going from $n = 1$ to $n = 2$ is about 1.8, but it is almost 5 when going from $n = 2$ to $n = 3$. Such a gap might be an indication of a large drop in the binding energy associated to the attachment of a third methanol molecule. Binding energies have been associated with both steric and electronic effects. They normally decrease as the cluster size increases, but transition metals seem to be an exception to the rule, especially for the binding of the first two ligands.

3.3. Copper with acetone

The mass spectrum with acetone as the seeded ligand is shown in Fig. 5. The mass spectrum was obtained using the channel-type nozzle of Fig. 3(a) with two copper electrodes. The discharge was done with a 0.2 μF capacitor charged to 1 kV. The concentration of acetone seeded in helium was less than 3% with a backing pressure of 1 atm. The spectrum looks very clean and only a few fragmentation ions of acetone show up. A peak at 43 u is assigned to $C_2H_3O^+$; another one at 59 u is assigned to protonated acetone. Two more impurity peaks at 91 and 105 u appear and are unassigned. The copper ion signal is rather large when compared with the Cu^+–(acetone)$_n$ signals for $n = 1$ and 2. This might be attributed to the low binding energy of the Cu^+–(acetone)$_n$ cluster and the small amount of ligand seeded into the carrier. It is likely that the charge is localized on the copper moiety in the complexes. This

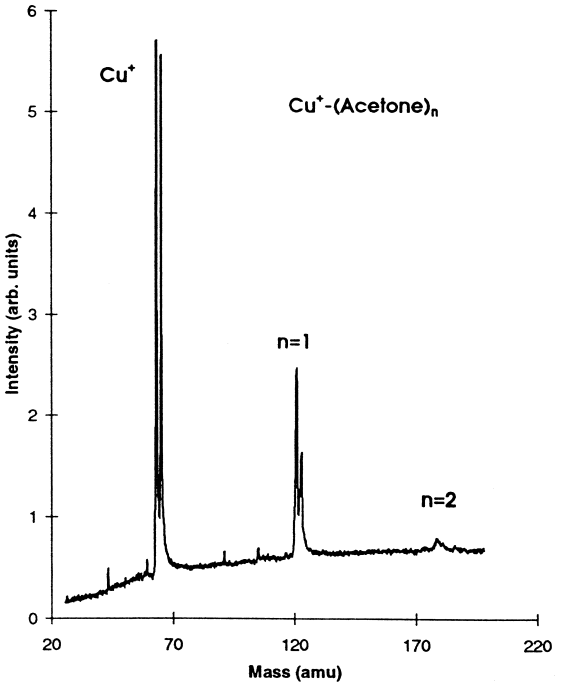

Fig. 5. Cluster mass spectrum of Cu^+–(acetone)$_n$. The ligated metal ion peaks corresponding to $n = 1$ and 2 are observed besides the Cu^+ isotopes at 63 and 65 u. Expansion conditions: less than 3% acetone in He, backing pressure 1 atm, channel-type nozzle [Fig. 3(a)] with Cu electrodes, discharge 0.2 μF/1 kV.

results in only small charge transfer interaction and therefore a weaker binding. Bond dissociation enthalpies are unavailable for the complex.

Copper ion is known to react with acetone under hydride or methanide abstraction. Insertion into the carbon frame work of ketones is not observed [25]. The lack of insertion reactions into ketones assures that the structure of the observed Cu^+–(acetone)$_n$ clusters is that of an adduct. Nothing can be said about the occurrence or absence of the hydride or methanide abstraction reactions under the high pressure in the expansion. All ion chemistry will most likely always be disguised by the expected complex processes occurring in the expansion channel. But it can be said that the desired product, the adduct of metal ion and seeded ligand, is formed in the expansion. There is no evidence of pure or protonated ligand clusters in the copper–acetone spectra.

In agreement with the results obtained using laser ablation [9,28], the reaction between acetone and copper (I) only yields the condensation products $Cu^+(CH_3COCH_3)_n$. Unfortunately, there is no evidence of intensity gaps because the signals from clusters with $n > 2$ are undetectable. Indeed, the amount of the $n = 2$ cluster seems to be very small with respect to the $n = 1$ cluster. As explained by the authors [9,28], this could be a result of the expansion conditions and not from low binding energies.

Another Cu^+–(acetone)$_n$ spectrum has been published by our group previously [29]. Different expansion conditions were used, and therefore larger signals were obtained. In this spectrum, signals from copper–acetone ion clusters with up to four acetone molecules are observed. An important feature is the difference in the intensities of the $n = 1$ and 2 when compared with the $n > 2$. The most interesting observation was the small effect observed in the intensities of the $n = 3$ and $n = 4$ cluster ions, when the different delay times between the firing of the discharge and the extraction pulse were examined. Both the $n = 1$ and $n = 2$ showed different intensity ratios depending on the delay time. The result suggests that the binding of more than two acetone molecules to a copper ion is much more difficult than one or two molecules. This behavior was explained in terms of a sudden decrease in the consecutive binding energies. This pattern is similar to that observed by water and ammonia condensation around a copper ion [14,26,27].

3.4. Copper with toluene

Fig. 6 shows a mass spectrum obtained with a channel-type nozzle of Fig. 3(a). The discharge was done with a 0.2 μF capacitor charged to 1 kV. The concentration of toluene seeded in helium was less than 5% with a backing pressure of 1 atm. Most of the copper ions are found to have one or two toluene molecules attached. The doublet of the ^{63}Cu and ^{65}Cu isotopes is still visible in the Cu^+–(toluene) cation complex.

The ion signal for toluene is small, considering the large amount of toluene in the expansion. This is a natural result of the charge exchange processes taking

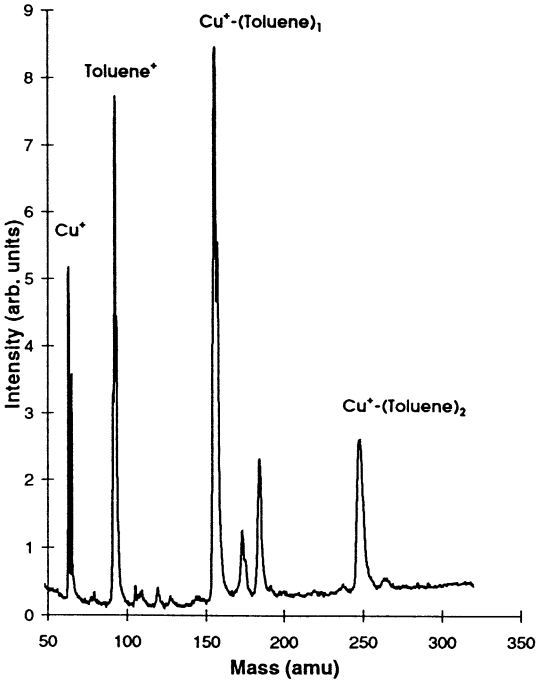

Fig. 6. Cluster mass spectrum of Cu^+–(toluene)$_n$. The ligated metal ion peaks corresponding to $n = 1$ and 2 are the major features besides the Cu^+ isotopes at 63 and 65 u, (toluene)$^+$ and the dimer ion of toluene. Expansion conditions: less than 5% toluene in He, backing pressure 1 atm, channel-type nozzle [Fig. 3(a)] with Cu cathode and graphite anode, discharge 0.2 μF/1 kV.

place in the expansion. Copper has an ionization potential of 7.726 eV, which is about 1 eV smaller than the 8.82 eV of toluene. The metal–ligand clusters can be expected to have even smaller ionization potentials than copper. Charge exchange produces the very desirable effect of transferring the ionization to the desired species. This, of course, will only be the case if the desired species have the lowest ionization potentials, but for metal–ligand clusters this is the case.

The dimer cation cluster of toluene is observed at 184 u, as well as a peak at 173 u. This is probably another complex of Cu due to the characteristic doublet structure, which is not resolved. The mass difference to the Cu^+–(toluene) peak at 155 u is 18 u. Water in the line from previous experiments might have therefore attached to the Cu^+–(toluene) cluster. Some other small features are also observed.

As can be seen from the mass spectra corresponding to copper–toluene, there are also some pure solvent clusters. In the copper–toluene mass spectrum, the predominant signal corresponds to the Cu^+–(toluene) cluster. This is due to the ion–molecule reaction of Cu^+ and toluene as found previously by Higashide et al. [8] using laser ablation. There is no evidence of clustering beyond $n = 2$, which suggests that the binding energies for more than two ligands are very low. Also, some toluene dimer can be observed in the mass spectrum (184 u). Pure toluene expansions produce toluene clusters by a condensation mechanism. Toluene cluster ions can be generated from direct ionization of the neutral cluster or by a charge transfer from the metal ions produced within the discharge.

3.5. Copper with water

The hydrated copper cations Cu^+–$(H_2O)_n$ are shown in Fig. 7. The clusters originate from using the pocket-type nozzle of Fig. 3(b) with copper electrodes. The discharge volume is separated from the expansion channel in this nozzle. Trials with a channel type nozzle of Fig. 3(a) did not produce satisfactory cluster ion signals for copper with water. At the same time it was also observed that the organic ligands discussed previously did not produce satisfactory results with the pocket discharge.

The intense Cu^+ doublet is followed by a series of hydrated species Cu^+–$(H_2O)_n$. The characteristic copper isotope doublet structure is clearly identified in each peak, even as the resolution decreases with mass. The hydrated clusters show a broad and only slowly decaying distribution. This is in contrast to what was observed so far for the organic ligand spectra. The most intense cation cluster is Cu^+–$(H_2O)_2$ and not Cu^+–(H_2O), as one might expect, but both possess more than twice the intensity of the clusters Cu^+–$(H_2O)_n$ with a $n > 2$. The integrated intensities in the range $n = 2$–6 are constant within the limits of uncertainty. A small series of peaks at 55, 73, 91, and 181 u is due to the protonated water clusters H^+–

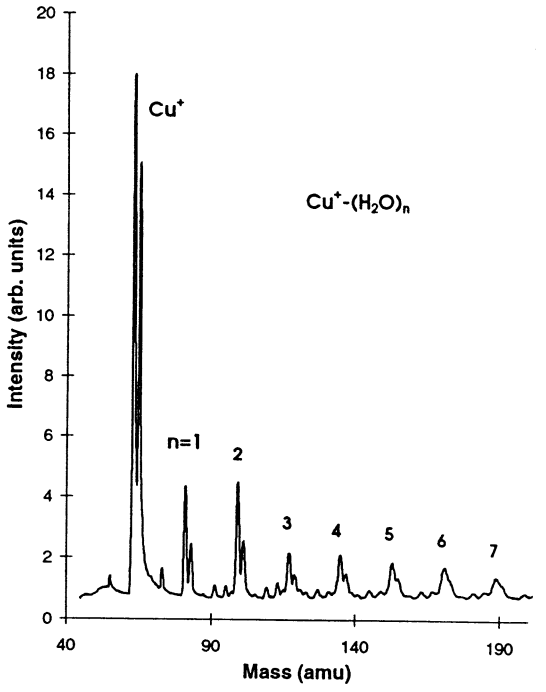

Fig. 7. Cluster mass spectrum of Cu^+–$(H_2O)_n$. The solvated metal ion peaks are observed for $n = 1$–7, besides the Cu^+ isotopes at 63 and 65 u. A number of impurity peaks appear due to line contamination. Expansion conditions: less than 2% water in He, backing pressure 1 atm, pocket-type nozzle [Fig. 3(b)] with Cu electrodes, discharge 0.2 μF/1.2 kV.

$(H_2O)_n$ with $n = 3$–10. Other peaks are due to contamination of the flow system.

The mechanism of protonated water clusters formation has been discussed in the literature [30], and it involves the condensation of water molecules around a hydronium (H_3O^+) ion. Both the copper ion and the metal–ligand cluster signals are stronger than those for the pure ligand. This suggests that most of the current from the discharge is used to ablate the metal from the electrode, and that the metal ion reacts promptly with the neutral water molecules to form the copper–water adducts. Only a small fraction of the current is used to generate hydronium ions, and therefore the amount of protonated water cluster is very small.

The spectrum in Fig. 7 agrees well with that presented by Magnera et al. [14] using fast atom bombardment of frozen metal. The most important coincidence is related to the distribution and relative intensities of the Cu^+–$(H_2O)_n$ clusters. In both spectra the $n = 2$ cluster ion shows an intensity larger than that for the $n = 1$ cluster. More important, there is a sudden drop in the intensity of the ion signals of the $n > 2$ clusters. Similarly to the results for organic ligands, this drop is attributed to the decrease in successive binding energies.

The successive hydration energies for the reaction: $Cu^+(H_2O)_{n-1} + H_2O \rightarrow Cu^+(H_2O)_n$ were determined by Holland and Castleman [13] for $n = 3$ and 4 using thermionic emission and by Magnera et al. [14] for the $n = 1$–4. The first and second hydration energies are very close (155 ± 17 and 159 ± 17 kJ/mol, respectively), whereas the third and fourth differ from them by a factor of ~2 (71 ± 8 and 67 ± 4 kJ/mol, respectively). Marinelli and Squires [26] found the same pattern for the hydrates of the first row transition metals ions V^+, Cr^+, Mn^+, Fe^+, Co^+, and Ni^+. Such behavior for transition metals differs from the binding energy pattern for the hydration of alkaline metal ions. Alkaline metal ions exhibit progressively decreasing binding energies for such ligands like water, ammonia, and other small molecules. Charge dispersal and intraligand steric effects increase with the addition of each new ligand reducing the interaction energies in the growing cluster ion [26].

The different behavior on the hydration of the transition metals is usually explained considering their electronic configuration and their ligand interaction. The presence of filled d orbitals plays an important role in the binding of any ligand when compared to the binding of ligands to alkaline metals. Transition metals have the ability to reduce metal–ligand repulsion by $sd\sigma$ hybridization due to the small energy difference between the 4s and 3d orbitals. This type of hybridization reduces the charge density along the σ axis increasing the binding energy of the second ligand. The reduction in the binding energy of a third ligand has been attributed to the loss of $sd\sigma$ hybridization [13]. Also, the effect of ligand to ligand repulsion becomes more important as the size of the cluster increases. Bausclicher et al. [31] have calculated the hydration energies of up to four water

ligands at the self-consistent-field (SCF) and modified coupled-pair functional (MCPF) levels. The best agreement with experiment was found at the MCPF level including electron correlation to account for the effects of the $sd\sigma$ hybridization. Their theoretical results (162, 165, 64, and 56 kJ/mol, for $n = 1$, 2, 3, and 4, respectively) agree well with the experimental trend. In their work, they also replaced the copper ion for a point charge. A good agreement was also obtained with the experimental values. Based on this, the authors concluded that the charge–dipole interactions and ligand–ligand repulsion are the main factors determining the binding energy. The large reduction between the second and third ligand binding energy is mainly due to the ligand–ligand repulsion and in a small extent to the loss of $sd\sigma$ hybridization.

3.6. Aluminum with water

The mass spectrum in Fig. 8 was recorded with a disc type nozzle of Fig. 3(c) employing aluminum electrodes. The two major series observed in the spectrum are the protonated water clusters H^+–$(H_2O)_n$ starting at 19 u ($n = 1$) and the hydrated aluminum cations Al^+–$(H_2O)_m$ starting at 45 u ($m = 1$). As mentioned above, sputtering from disc-type nozzles was never observed to be very intense. Therefore most of the discharge current goes into the production of hydronium ions, which forms adducts with neutral water molecules.

A very weak series 59, 77, 95, and 113 u is assigned as AlO_2^+–$(H_2O)_m^+$, $m = 1$, 2, 3, and 4, respectively. Another weak series 51, 69, 87, and 105 u appears and is attributed to AlO^+–$(H_2O)_m$ with $m = 1$, 2, 3, and 4. There is a quite strong signal at 32 and 16 u, due to molecular and atomic oxygen. The oxygen is produced by decomposition of H_2O in the discharge. The ionization potential of O_2 is 12.1 eV and is similar to the 12.5 eV of H_2O. The O_2 ionization might be a little enhanced by charge exchange with the abundant H_2O^+. Usually H_2O^+ is not detected in the cluster mass spectra of water because it reacts fast with excess water to H_3O^+ and OH.

The observation of H_2O^+ indicates that at least some ionization occurs a few nozzle diameters away from the throat, where the number density of H_2O is small and the reaction does not occur. The structure of the Al^+–(H_2O) is most likely that of the adduct and not the protonated hydroxide $(AlOH)H^+$. Evidence for this is the ready exchange of H_2O against stronger bases (alcohols) [32]. So the definite structure can only be deduced by a spectroscopic interrogation as was done for $V(H_2O)^+$ where the adduct structure was found [33].

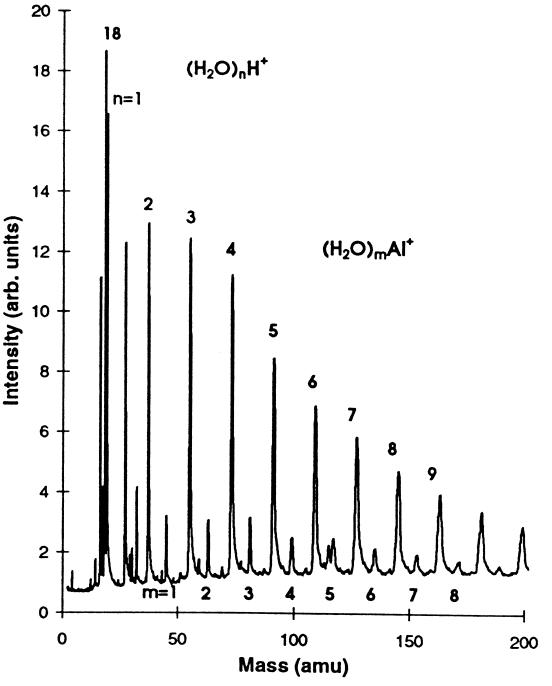

Fig. 8. Cluster mass spectrum of Al^+–$(H_2O)_n$. The solvated metal ion peaks are observed interlacing the intense $(H_2O)_nH^+$ clusters. Expansion conditions: less than 2% water in He, backing pressure 1 atm, disc-type nozzle [Fig. 3(c)] with Al electrodes, discharge 0.2 μF/1 kV.

Uppal and Staley [32] detected the formation of aluminum–water clusters when studying the reaction of aluminum (I) and alcohols. However, water was always exchanged by alcohol, which is a stronger base. The main products of the aluminum ion and water reaction observed in our spectrum are Al^+–$(H_2O)_m$ clusters in which $m = 1$–9 could be detected. An analysis of the integrated intensities suggests an intensity gap in going from the $m = 3$ to $m = 4$

cluster, although it is very small. Direct comparison with aluminum–water cluster spectra from the literature was not possible.

Some other mass spectra of aluminum–ligand clusters have been reported in the literature. They involve the production of aluminum ion by laser ablation and the reaction of it with ligands such as ammonia [34], benzene [35], isobutylene and tert-butyl chloride [36] and water–ammonia mixtures [37].

When ammonia is used as the ligand [34] the main product is the condensation of ammonia around the metal ion Al^+–$(NH_3)_n$. The extent of clustering observed was large as cluster ions of $n = 15$ were observed. An intensity gap in going from the third ligand to the fourth was found.

When benzene was used as a ligand [35] the condensation reaction to produce Al^+–$(C_6H_6)_n$ was found to be the only one. The extent of clustering was smaller than that for NH_3 as noticed by the presence of ion signals only for $n = 1$–4.

When isobutylene is used [36], the predominant signal corresponds to condensation of isobutylene around the metal ion, although some other reaction products are also observed. The spectrum is dominated by the Al^+–(isobutylene) cluster and an intensity gap seems to be occurring in the $n = 2$ to $n = 3$ transition. A more interesting result is observed when tert-butyl chloride is used [36]. The spectrum is dominated by isobutane-tert butyl chloride clusters. These result from the transfer of chloride to the metal ion [32]. However, there are also signals corresponding to the condensation of the alkane chloride around the metal ion. Both the $n = 3$ and $n = 4$ give the more intense signals, suggesting that they might be more stable than the $n = 1$ and 2 structures.

Exposure to a mixture of water and ammonia [37] gave interesting results. There were no pure aluminum–water ion clusters in the spectrum, although pure aluminum–ammonium could be seen. Also mixed $Al^+(NH_3)_m(H_2O)_n$ were observed in smaller amounts. Another important feature is that an intensity gap at $n + m = 3$ was observed, independent of the ligand. Based on these results, the authors suggested that Al^+ is able to accommodate three ligands in its first coordination sphere, and that there is a tendency to favor ammonia ligands. Our results compare well with the reports mentioned above. A small intensity gap is detected after the $n = 3$ aluminum–water cluster ion in our spectrum.

Similarly to the results for the copper–ligand ion clusters, the signal distribution of the mass spectrum reflects the behavior of the binding energies. Theoretical calculations of the binding energies for water and aluminum (I) ion have been done by Bauschlicher and Partridge [38] and Watanabe et al. [39]. The first group used ab initio calculation at the 6-31G* level and obtained 120, 96, 81, and 75 kJ/mol as the values of successive binding energies for $n = 1$–4, respectively. The second group used Hartree-Fock, second order Møller-Plesset and fourth order Møller-Plesset single, double, triple, and quadruple (MP4SDTQ) levels to obtain values (150, 121, 105, 105, 100 kJ/mol for $n = 1$–5, respectively, at the MP4SDTQ level) which differ from the ones mentioned previously. Although different, the results have the same characteristic trends. The binding energy decreases almost linearly for the first three water molecules and levels off after three molecules have been reached. Both groups concluded that the aluminum (I) cation binds three ligand molecules at its first coordination sphere. At $n = 4$ a second coordination sphere starts where the fourth ligand binds two water molecules by hydrogen bonds forming a six membered ring together with the aluminum ion.

These results differ from those obtained for transition and alkaline metals [38]. The differences can be explained in terms of the electronic distribution of the metal ion. Al^+ has an occupied 3*s* orbital contrary to the corresponding alkaline metal ion (Na^+), and it does not have electrons in the *d* orbital as the transition metals do. Hybridization of the 3*s* and 3*p* orbitals after binding of the first ligand is the most important effect for the behavior of the aluminum (I) ion. Such hybridization induces the polarization of the 3*s* orbital which enhances the bonding of the first ligand, but makes the binding of a second ligand less favorable. Because of this polarization, the second ligand has to approach the metal from the first ligand side, increasing the effect of the ligand–ligand repulsion in the binding energy. On the contrary, for

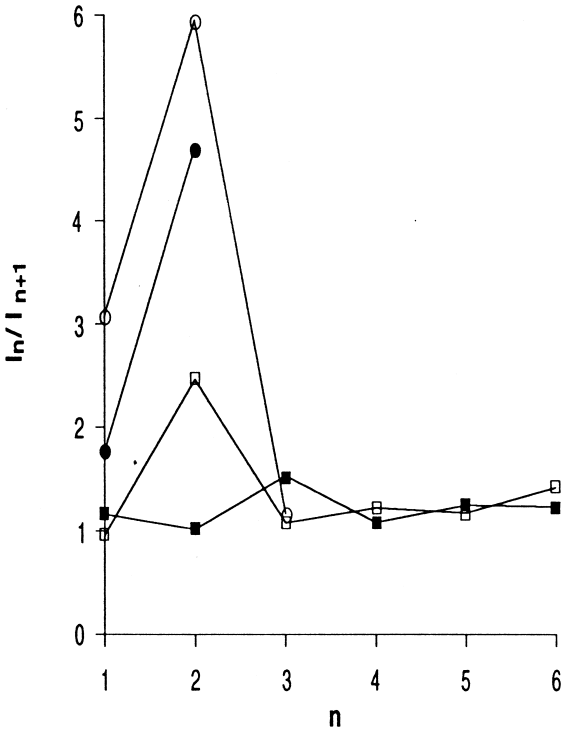

Fig. 9. Intensity changes for metal–ligand ion clusters M^+L_n. Breaks indicate an intensity gap at the cluster number n. (closed square) $Al^+(H_2O)_n$; (open square) $Cu^+(H_2O)_n$; (open circle) $Cu^+(acetone)_n$ from [29]; (closed cirlce) $Cu^+(methanol)_n$.

alkaline and transition metals, the approach of the second ligand occurs opposite to the first ligand location. In alkaline metal the polarization is small, while in transition metals the hybridization is different. What seems more important is that the hybridization and polarization of the 3*s* level in Al^+ seems to largely reduce the ligand–ligand repulsion when a third molecule approaches. As a result, a more stable ion cluster results when $n = 3$.

3.7. Comparison of the metal–ligand ion clusters

Fig. 9 shows the changes in intensity of the clusters by plotting the ratio of the intensities for the n and the $n + 1$ copper ion clusters with water, acetone, and methanol. The aluminum–water results are also shown.

Considering the copper–ligand ion clusters, there seems to be an agreement in how the binding of the ligands to the metal ion occurs. Both the first and second ligand molecules attach promptly to the metal, whereas the binding of extra ligand molecules is more difficult. After $n = 2$ the size of the ligand becomes a very important factor, as the ligand–ligand repulsion (steric hindrance) seems to be the more influential factor in the binding process. This can be seen when both the copper–water and the copper–toluene ion cluster mass spectra are considered. The extent of clustering with water is much larger ($n = 1$–7) than that for toluene ($n = 1$–2). The larger size of the toluene molecules will probably make the binding energy for the third and consecutive toluene molecules smaller than those reported for water binding.

A comparison can also be made between two different metals (Cu^+ and Al^+) reacting with the same ligand. As seen in Fig. 9, there is a large drop in intensity going from $n = 2$ to $n = 3$ in the copper–water ion cluster spectrum, whereas for aluminum–water this occurs at the $n = 3$ to $n = 4$ transition. This was explained in terms of the difference in electronic distribution and orbital hybridization of the metal, which results in different spatial arrangements of the ligands around the ion core. For the copper (I) ion the binding of a second molecule is easy due to the $sd\sigma$ hybridization. The attachment of a third ligand is more difficult mainly due to ligand to ligand repulsion. This is reflected in the consecutive binding energies, which are almost equal for the first two water molecules, but decreases largely for successive water molecules. For aluminum, *sp* hybridization makes the repulsive interaction between the two first water molecules determine the binding energy of the second ligand. However, the same hybridization stabilizes the approach of a third molecule by minimizing the interaction between the ligands. After $n = 3$ the binding energies are almost the same as the new ligands bind to other water molecules and not to the metal.

4. Conclusion

The examples presented show that it is possible to form metal–ligand ion complexes by pulsed discharge

ionization in a jet. The metal is provided by ablation of electrode material by the discharge. Ablation of enough electrode material can be achieved under modest discharge conditions (0.2 μF/1 kV typically corresponding to 0.1 J/shot).

The characteristic of the discharge ionization process under high pressures, to shift the ionization by charge exchange processes to the species with the lowest ionization potentials, guarantees a high ionization yield of the metal containing species and is of advantage for the application. When swamping the spectrum with orders of magnitude, the larger monomer or carrier gas signals are not observed. Any ligand that can be seeded in a high enough concentration seems to be attachable to a metal cation to produce the adduct complex.

The flow of the ligands through the discharge does not create fundamental problems with either the discharge operation or ligand destruction. Tested were water, methanol, acetone, ethylether, toluene, and benzene. Compounds representative for large classes of substances. Clusters containing fragments of the ligand and a ligand molecule are rarely detected.

Conditions seem to be adjustable in most cases to produce metal ion–ligand complexes as the dominating ionic species. The changes in the successive binding energies of ligands can be observed in the cluster ion mass spectra by step formation. This was shown for Cu^+–$(H_2O)_n$ where binding energy data are available. The same behavior of the successive binding energies as found for copper water cluster ions is indicated for Cu^+–$(acetone)_n$ cluster ions by the changes observed in the mass spectra. A bracketing technique for metal–ligand binding energies might be feasible by expansion of several ligands with a single metal or several metals with single ligand.

Acknowledgements

This work was supported by the Robert A. Welch Foundation under grant no. AA-1173. The authors thank Larry G. White and John C. Simcik III from the Laser Electro-Optics and Vacuum Technology Programs at Texas State Technical College of Waco (TSTC) for their contribution in building the vacuum system for the molecular beam apparatus. They also thank Milton L. Luedke for machining numerous parts for our vacuum system and Jerry M. Milner for repair and construction of electronic equipment.

References

[1] T.G. Dietz, M.A. Duncan, D.E. Powers, R.E. Smalley, J. Chem. Phys. 74 (1981) 6511.
[2] V.E. Bondybey, J.H. English, J. Chem. Phys. 74 (1981) 6978.
[3] D.S. Cornett, M. Peschke, K. LaiHing, P.Y. Cheng, K.F. Willey, M.A. Duncan, Rev. Sci. Instrum. 63 (1992) 2177.
[4] K. LaiHing, R.G. Wheeler, W.L. Wilson, J. Chem. Phys. 87 (1987) 3401.
[5] H. Haberland, Clusters of Atoms and Molecules, H. Haberland (Ed.), Springer Series in Chemical Physics, Vol. 52, Springer, Berlin, 1994, Chap. 3.
[6] H.R. Siekmann, Ch. Lueder, J. Faehrmann, H.O. Lutz, K.H. Meiwes-Broer, Z. Phys. D. 20 (1991) 417.
[7] G. Gantefoer, H.R. Siekmann, H.O. Lutz, K.H. Meiwes-Broer, Chem. Phys. Lett. 165 (1990) 293.
[8] H. Higashide, T. Oka, K. Kasatani, H. Shinohara, H. Sato, Chem. Phys. Lett. 163 (1989) 485.
[9] R.C. Burnier, G.D. Byrd, B.S. Freiser, Anal. Chem. 52 (1980) 1641.
[10] R.W. Jones, R.H. Staley, J. Phys. Chem. 86 (1982) 1669.
[11] D.A. Weil, C.L. Wilkins, J. Am. Chem. Soc. 107 (1985) 7316.
[12] M.S. El-Shall, K.E. Schriver, R.L. Whetten, M. Meot-Ner, J. Phys. Chem. 93 (1989) 7969.
[13] P.M. Holland, A.W. Castleman Jr., J. Chem. Phys. 76 (1982) 4195.
[14] T.F. Magnera, D.E. David, D. Stulik, R.G. Orth, H.T. Jonkman, J. Michl, J. Am. Chem. Soc. 111 (1989) 5036.
[15] K.F. Willey, C.S. Yeh, D.L. Robins, M.A. Duncan, J. Phys. Chem. 96 (1992) 9106.
[16] C.T. Scurlock, S.H. Pullins, J.E. Reddic, M.A. Duncan, J. Chem. Phys. 104 (1996) 4591.
[17] K.F. Willey, C.S. Yeh, D.L. Robins, J.S. Pilgrim, M.A. Duncan, J. Chem. Phys. 97 (1992) 8886.
[18] M.H. Shen, J.M. Farrar, J. Phys. Chem. 93 (1993) 4386.
[19] M.H. Shen, J.M. Farrar, J. Chem. Phys. 94 (1991) 3322.
[20] J.M. Farrar, Cluster Ions, C.Y. Ng, T. Baer, I. Powis (Eds.), Wiley, New York, 1993, p. 243.
[21] C.J. Weinheimer, J.M. Lisy, J. Chem. Phys. 105 (1996) 2938.
[22] C.J. Weinheimer, J.M. Lisy, Int. J. Mass Spectrom. Ion Processes 159 (1996) 197.
[23] T. J. Selegue, J.M. Lisy, J. Phys. Chem. 96 (1992) 4143.
[24] W. Liu, J.M. Lisy, J. Chem. Phys. 89 (1988) 605.
[25] T. Kaya, Y. Horiki, M. Kobayashi, H. Shinohara, H. Sato, Chem. Phys. Lett. 200 (1992) 435.
[26] P.J. Marinelli, R.R. Squires, J. Am. Chem. Soc. 111 (1989) 4101.
[27] T. Kaya, M. Kobayashi, H. Shinohara, H. Sato, Chem. Phys. Lett. 186 (1991) 431.

[28] R.C. Burnier, G.D. Byrd, B.S. Freiser, J. Am. Chem. Soc. 103 (1981) 4360.
[29] A. Brock, D.L. Cedeño, C. Manzanares I., Rev. Sci. Instrum. 69 (1998) 2331.
[30] J.Q. Searcy, J.B. Fenn, J. Chem. Phys. 61 (1974) 5282.
[31] C.W. Bauschlicher Jr., S.R. Langhoff, H. Partridge, J. Chem. Phys. 94 (1991) 2068.
[32] J.S. Uppal, R.H. Staley, J. Am. Chem. Soc. 104 (1982) 1229.
[33] D.E. Lessen, R.L. Asher, P.J. Brucat, J. Chem. Phys. 93 (1990) 6102.
[34] T. Kaya, M. Kobayashi, H. Shinohara, H. Sato, Chem. Phys. Lett. 186 (1991) 431.
[35] H. Higashide, T. Kaya, M. Kobayashi, H. Shinohara, H. Sato, Chem. Phys. Lett. 171 (1990) 297.
[36] G.M. Daly, M.S. El-Shall, J. Phys. Chem. 99 (1995) 5283.
[37] O. Ito, Y. Horiki, S. Nishio, A. Matsuzaki, H. Sato, Chem. Lett. 1 (1995) 9.
[38] C.W. Bauschlicher, H. Partridge, J. Phys. Chem. 95 (1991) 9694.
[39] H. Watanabe, M. Aoki, S. Iwata, Bull. Chem. Soc. Jpn. 66 (1993) 3245.